THE JOURNAL OF BIOLOGICAL CHEMISTRY
Vol. 278, No. 51, Issue of December 19, pp. 51176–51183, 2003
Printed in U.S.A.

Inhibition of Fructose-1,6-bisphosphatase by a New Class of Allosteric Effectors*

Received for publication, July 31, 2003, and in revised form, October 3, 2003
Published, JBC Papers in Press, October 6, 2003, DOI 10.1074/jbc.M308396200

Jun-Young Choe‡, Scott W. Nelson‡, Kristen L. Arienti§¶, Frank U. Axe§¶, Tassie L. Collins§‖, Todd K. Jones§¶, Rachel D. A. Kimmich§, Michael J. Newman§‡‡, Karl Norvell§, William C. Ripka§ §§, Suzanne J. Romano§, Kevin M. Short§¶, Deborah H. Slee§, Herbert J. Fromm‡, and Richard B. Honzatko‡¶¶**

From the ‡Department of Biochemistry, Biophysics, and Molecular Biology, Iowa State University, Ames, Iowa 50011 and §Ontogen Corp., Carlsbad, California 92009

A highly constrained pseudo-tetrapeptide (OC252–324) further defines a new allosteric binding site located near the center of fructose-1,6-bisphosphatase. In a crystal structure, pairs of inhibitory molecules bind to opposite faces of the enzyme tetramer. Each ligand molecule is in contact with three of four subunits of the tetramer, hydrogen bonding with the side chain of Asp^{187} and the backbone carbonyl of residue 71, and electrostatically interacting with the backbone carbonyl of residue 51. The ligated complex adopts a quaternary structure between the canonical R- and T-states of fructose-1,6-bisphosphatase, and yet a dynamic loop essential for catalysis (residues 52−72) is in a conformation identical to that of the T-state enzyme. Inhibition by the pseudo-tetrapeptide is cooperative (Hill coefficient of 2), synergistic with both AMP and fructose 2,6-bisphosphate, noncompetitive with respect to Mg^{2+}, and uncompetitive with respect to fructose 1,6-bisphosphate. The ligand dramatically lowers the concentration at which substrate inhibition dominates the kinetics of fructose-1,6-bisphosphatase. Elevated substrate concentrations employed in kinetic screens may have facilitated the discovery of this uncompetitive inhibitor. Moreover, the inhibitor could mimic an unknown natural effector of fructose-1,6-bisphosphatase, as it interacts strongly with a conserved residue of undetermined functional significance.

Fructose-1,6-bisphosphatase (D-fructose-1,6-bisphosphate 1-phosphohydrolase, EC 3.1.3.11; FBPase)[1] catalyzes a tightly regulated step of gluconeogenesis, the hydrolysis of fructose 1,6-bisphosphate ($F16P_2$) to fructose 6-phosphate (F6P) and P_i (1, 2). AMP and $F26P_2$ (binding to allosteric and active sites, respectively) inhibit FBPase, while simultaneously activating its counterpart in glycolysis, fructose-6-phosphate 1-kinase (3, 4). Biosynthesis and degradation of $F26P_2$ is subject to hormonal control principally by glucagon and insulin (4, 5). $F26P_2$ enhances the binding of AMP to FBPase by up to an order of magnitude (6). Hence, although intracellular concentrations of AMP remain relatively constant, AMP becomes a more potent inhibitor of FBPase as concentrations of $F26P_2$ increase. AMP binds 28 Å away from the nearest active site and perhaps not surprisingly inhibits catalysis noncompetitively with respect to $F16P_2$. Yet AMP is a competitive inhibitor of catalysis with respect to essential divalent cations (Mg^{2+}, Mn^{2+}, or Zn^{2+}), all of which are in proximity to (and probably coordinate with) the 1-phosphoryl group of $F16P_2$ (7−10).

FBPase is a homotetramer (subunit M_r of 37,000 (11)) and exists in at least two distinct quaternary conformations called R and T (12−14). AMP induces the transition from the active R-state to the inactive (or less active) T-state. Substrates or products in combination with metal cations stabilize the R-state conformation. A proposed mechanism for allosteric regulation of catalysis involves three conformational states of loop 52−72 called engaged, disengaged, and disordered (15). AMP alone or with $F26P_2$ stabilizes a disengaged loop (16, 17), whereas metals with products stabilize an engaged loop (10, 17−19). In active forms of the enzyme, loop 52−72 probably cycles between its engaged and disordered conformations (15, 18). Fluorescence from a tryptophan reporter group at position 57 is consistent with the conformational states for loop 52−72, observed in crystal structures (20, 21). Presumably, the engaged, disengaged, and disordered conformations of loop 52−72 are possible in both the R- and T-states of FBPase, but only the engaged and disordered conformers of the R-state, and the disengaged conformer of the T-state, have been reported in crystalline complexes (17, 18, 22, 23).

A recent report (24) in the literature identifies a new inhibitor site on FBPase, distinct from the active and the AMP-binding sites. The new family of anilinoquinazoline inhibitors was discovered by a search for potential drugs in the treatment of non-insulin-dependent diabetes. Although the site of binding on FBPase is clear, the kinetic mechanism of inhibition for this new class of inhibitor was not reported. Independent of the efforts above, a screen for new inhibitors of FBPase resulted in the discovery of a chemically distinct molecule (OC252–324,

* This work was supported in part by National Institutes of Health Research Grant NS 10546, Small Business Innovation Research Grants R43 DK57342-01 (phase 1) and R44 DK57342-02 (phase 2), and Dr. Barry Toyonaga, Ontogen Corp. The costs of publication of this article were defrayed in part by the payment of page charges. This article must therefore be hereby marked "*advertisement*" in accordance with 18 U.S.C. Section 1734 solely to indicate this fact.

The atomic coordinates and structure factors (code 1Q9D) have been deposited in the Protein Data Bank, Research Collaboratory for Structural Bioinformatics, Rutgers University, New Brunswick, NJ (http://www.rcsb.org/).

¶ Present address: Johnson & Johnson Pharmaceutical Research and Development, L. L. C., 3210 Merryfield Row, San Diego, CA 92121.

‖ Present address: Tularik Inc., 1120 Veterans Blvd., South San Francisco, CA 94080.

** Present address: Dihedron Corp., 10931 North Torrey Pines Rd., Ste. 104, La Jolla, CA 92037.

‡‡ Present address: Ferring Research Institute Inc., 3550 General Atomics Court, San Diego, CA 92121.

§§ Present address: Cheminomics Group, 10819 Red Rock Dr., San Diego, CA 92131.

¶¶ To whom correspondence should be addressed. Tel.: 515-294-6116; Fax: 515-294-0453; E-mail: honzatko@iastate.edu.

[1] The abbreviations used are: FBPase, fructose-1,6-bisphosphatase; $F16P_2$, fructose 1,6-bisphosphate; F6P, fructose 6-phosphate; $F26P_2$, fructose 2,6-bisphosphate.

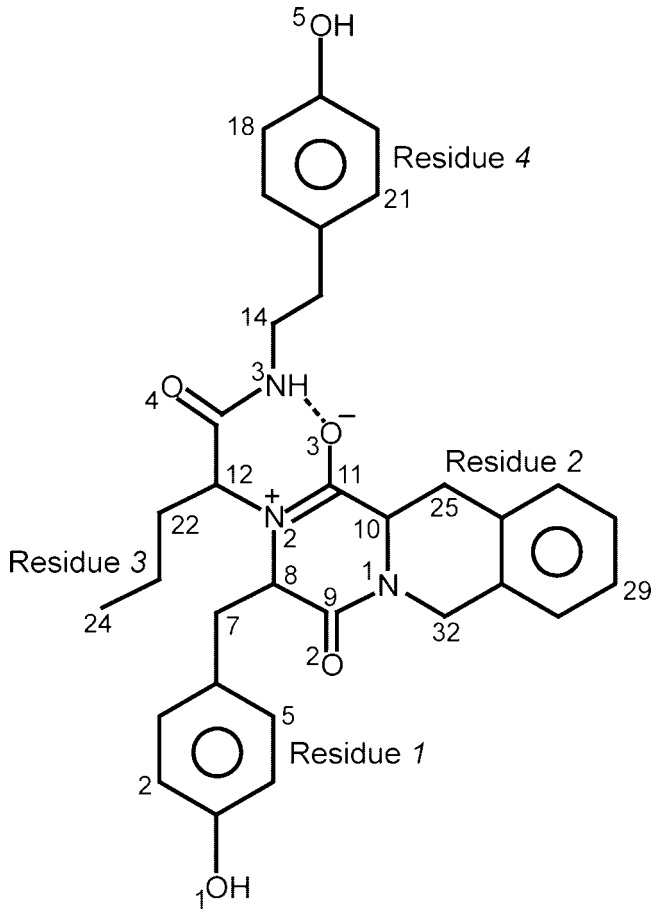

FIG. 1. **Covalent structure of OC252.** Atoms C-8, C-10, C-12, and C-14 correspond to Cα atoms of residues labeled *1*–*4*. Atoms C-8, C-10, and C-12 adopt the L-configuration of a common amino acid. *Residues 1* and *4* have tyrosyl side chains; *residue 2* has a phenylalanine side chain bridged by a methylene group to its amide nitrogen atom (N-1), and *residue 3* has an *n*-propyl side chain. In its crystalline complex, a close contact between atoms N-3 and O-3 infers a strong intramolecular hydrogen bond. The electronic resonance state of the bond between atoms N-2 and C-11 is speculative but would account for the close contact between backbone carbonyl 51 (from FBPase) and atom N-2 through enhanced electrostatic interactions.

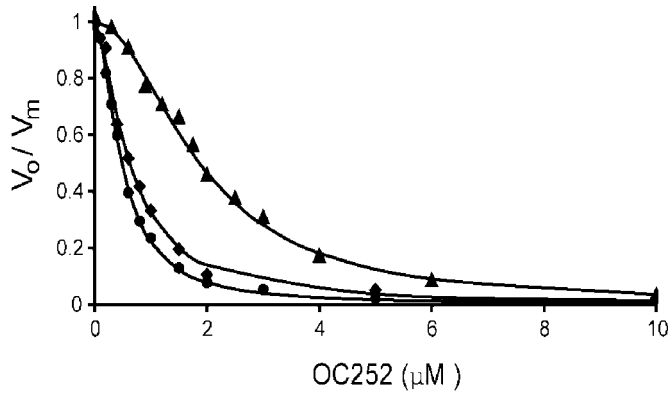

FIG. 2. **Synergism in the inhibition of FBPase by OC252, F16P_2, and AMP.** OC252 concentrations vary from 0 to 10 μM. *Symbols* represent relative velocities for OC252 alone (▲), OC252 with 0.45 μM F26P_2 (♦), and OC252 with 1.5 μM AMP (●). Assays use 50 mM Hepes, pH 7.5, with 0.5 mM $MgCl_2$ and 20 μM F16P_2. Curves are fits to the data using Equation 1.

hereafter OC252, Fig. 1) that targets the same binding site on FBPase. Inhibition of FBPase by OC252 is cooperative (Hill coefficient of 2), synergistic with AMP and F26P_2, noncompetitive with respect to Mg^{2+}, but uncompetitive with respect to F16P_2. OC252 greatly decreases the concentration at which substrate inhibition dominates the kinetics of FBPase. The crystal structure reveals a pair of OC252 molecules bound to each face of an FBPase tetramer. The quaternary conformation of the tetramer differs from the canonical R- and T-states, observed in the absence and presence of AMP, respectively, yet the loop (residues 52–72) is in its disengaged conformation. A strong hydrogen bond between OC252 and the side chain of a conserved aspartate residue of undetermined functional significance suggests the possibility of a binding site recognized by an unknown natural effector.

EXPERIMENTAL PROCEDURES

Materials—F16P_2, F26P_2, $NADP^+$, and AMP were purchased from Sigma. Glucose-6-phosphate dehydrogenase and phosphoglucose isomerase came from Roche Applied Science. Other chemicals were of reagent grade or the equivalent. QSW-HR high pressure liquid chromatography resin came from Toso-Hass Bioseparations. FBPase-deficient *Escherichia coli* strain DF 657 came from the Genetic Stock Center at Yale University. Plasmids used in the expression of wild-type FBPase came from a previous investigation (20). The inhibitor OC252 was provided by Ontogen Corp. (Carlsbad, CA).

Expression and Purification of Wild-type FBPase—Separate preparations of enzyme were used for the structural and kinetics investigations. Recombinant FBPase was expressed in a strain of *E. coli* deficient in endogenous FBPase and then purified to homogeneity. Cell-free extracts of the wild-type FBPases were subjected to heat treatment (65 °C for 5 min), followed by centrifugation. For enzyme used in kinetics investigations, the supernatant solution was loaded onto a Cibacron Blue-Sepharose column, previously equilibrated with 20 mM Tris-HCl, pH 7.5. FBPases were eluted from that column with 1 mM AMP and 20 mM Tris-HCl, pH 7.5. The eluent from the first column was loaded directly onto a DEAE-Sepharose column and then eluted with a NaCl gradient (0–0.3 M). The purified enzyme was dialyzed extensively against 20 mM Tris-HCl, pH 7.5. For crystallization experiments, after volume reduction by pressure concentration through an Amicon PM-30 membrane, the supernatant solution from centrifugation was passed through a CM-Sepharose column using a NaCl gradient (20–400 mM) in 10 mM Tris malonate, pH 6.0, and then dialyzed against KP_i (20 mM, pH 7.0). Purity and protein concentrations of FBPase preparations were confirmed by SDS-PAGE (25) and the Bradford assay (26), respectively.

Kinetic Experiments—Assays for the determination of specific activity, k_{cat}, and activity ratios at pH 7.5 and 9.5 employed the coupling enzymes, phosphoglucose isomerase and glucose-6-phosphate dehydrogenase (1). The reduction of $NADP^+$ to NADPH was monitored by absorbance spectroscopy at 340 nm. All other assays used the same coupling enzymes, but monitored NADPH production by its fluorescence emission at 470 nm, using an excitation wavelength of 340 nm. Kinetic assays were performed at room temperature (22 °C). Data fitting and analysis used the program DYNAFIT (27).

Crystallization of the Product Complex—Crystals of FBPase grew by the method of hanging drops. Equal parts of a protein solution (FBPase (10 mg/ml), KP_i, pH 7.4 (10 mM), $MgCl_2$ (5 mM), F6P (5 mM), and OC252 (2 mM)) and a precipitant solution (Tris malonate, pH 7.4 (2.5 mM), polyethylene glycol 3350 (6% w/v)) were combined in a droplet of 4 μl total volume. Wells contained 500 μl of the precipitant solution. Crystals of dimensions 0.4 × 0.4 × 0.3 mm grew in approximately 3 days at 20 °C. OC252 is relatively insoluble in aqueous solutions. Approximately 10 mg of pure inhibitor was dissolved initially in acetone, and appropriately measured aliquots were distributed to empty vials. The acetone was removed by evaporation, and the protein solution above was added. The inhibitor dissolved after a brief time interval to provide the clear protein solution used in the crystallization experiments.

Data Collection—Data were collected at Iowa State University on a rotating anode/Siemens area detector at 120 K, using CuK_α radiation passed through a graphite monochromator. Data were reduced by XENGEN (28).

Structure Determination, Model Building, and Refinement—Crystals grown for the present study are isomorphous to the AMP-Zn^{2+}-product complex (17). Phase angles, used in the generation of initial electron density maps, were based on model 1EYJ of the Protein Data Bank, from which water molecules, metal cations, small molecule ligands, and residues 52–72 had been omitted. Residues 52–72 were built into the electron density of omit maps, with reference to the Cα coordinates of loop 52–72 from the AMP complex (17), using the program XTALVIEW

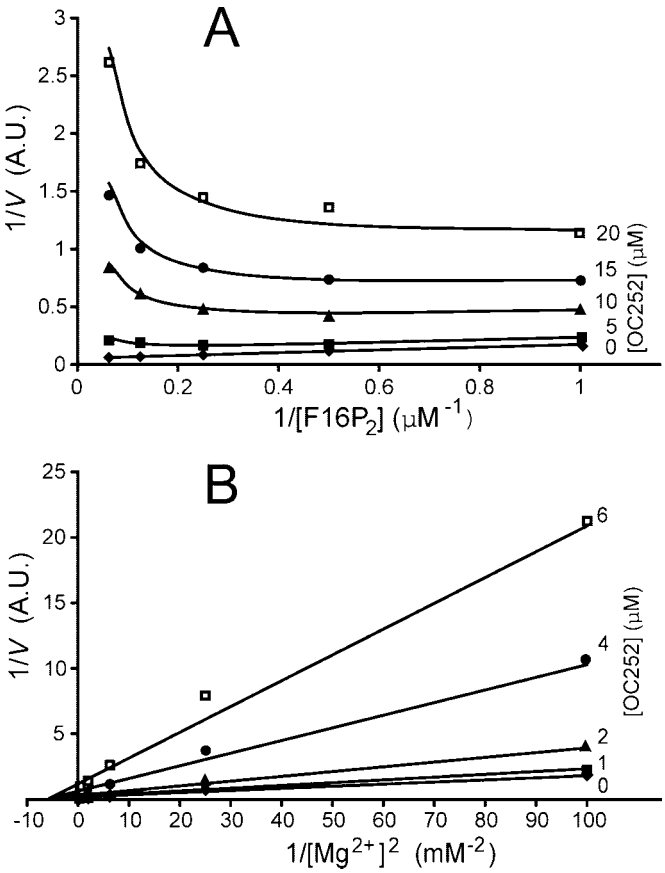

FIG. 3. **Kinetic mechanism of inhibition of FBPase by OC252.** *A,* data are taken at 1−20 μM $F16P_2$ in 50 mM Hepes, pH 7.5, with 5 mM $MgCl_2$. Curves are fits to the data using Equation 3. *B,* data are taken at 0.1−5 mM Mg^{2+} (corrected for chelation by EDTA) in 50 mM Hepes, pH 7.5, with 20 μM $F16P_2$. Curves are fits to the data using Equation 4.

(29) and a Silicon Graphics work station. A molecule of P_i and of F6P and two magnesium cations were added to omit electron density of the active site. Strong electron density remained, however, near the center of the tetramer, which easily accommodated a molecule of OC252. The resulting model underwent refinement, using CNS (30) with force constants and parameters of stereochemistry from Engh and Huber (31). A cycle of refinement consisted of slow cooling from 2500 to 300 K in steps of 25 K, followed by 120 cycles of conjugate gradient minimization, and concluded by the refinement of individual thermal parameters. Thermal parameter refinement employed restraints of 1.5 Å^2 on nearest neighbor and next-to-nearest neighbor main chain atoms, 2.0 Å^2 on nearest neighbor side chain atoms, and 2.5 Å^2 on next-to-nearest neighbor side chain atoms.

In subsequent cycles of refinement, water molecules were fit to difference electron density of 2.5σ or better and were added until no significant decrease was evident in the R_{free} value. Included in the final model were water molecules that make suitable donor-acceptor distances to each other and the protein and have thermal parameters under 60 Å^2.

RESULTS

Expression and Purification of Wild-type FBPase—Expression and isolation procedures described above provide FBPase in at least 95% purity, as judged by SDS-PAGE (data not shown). The k_{cat} value (22 ± 1 s^{-1}) and the ratio of specific activities at pH 7.5 to 9.5 (3.3) indicate high purity and little or no proteolysis of the purified enzyme, consistent with the results from electrophoresis.

Kinetics Experiments—By using fixed concentrations of $MgCl_2$ (0.5 mM, approximately the K_a for Mg^{2+}) and $F16P_2$ (20 μM, saturating), initial velocities vary as the inverse square of OC252 concentration (Hill coefficient of 1.97 ± 0.1) with an $I_{0.5}$ (concentration of OC252 that causes 50% inhibition) of 1.87 ± 0.07 μM (Fig. 2). $F26P_2$, AMP, and OC252 inhibit FBPase synergistically; $I_{0.5}$ values for OC252 are 0.63 ± 0.04 μM (Hill coefficient, 1.6 ± 0.1) in the presence of 1.5 μM AMP and 0.48 ± 0.01 μM (Hill coefficient, 1.7 ± 0.1) in the presence of 0.45 μM $F26P_2$. The numerical values above result from a fit of data to Equation 1,

$$V_o/V_m = I_{0.5}/(I_{0.5} - I^n) \quad \text{(Eq. 1)}$$

where n is the Hill coefficient, V_m the initial velocity in the absence of inhibitor, V_o the initial velocity at a specific inhibitor concentration, I the concentration of OC252, and $I_{0.5}$ the concentration of OC252 that causes 50% inhibition.

Kinetics data were taken over broad concentration ranges of Mg^{2+} (0.2−5 mM), $F16P_2$ (1−20 μM), and OC252 (0−20 μM) in order to determine the kinetic mechanism of inhibition. Plots of reciprocal velocity against $1/[Mg^{2+}]^2$ ($F16P_2$ saturating, but below concentrations that cause significant substrate inhibition) and $1/[F16P_2]$ (Mg^{2+} saturating) indicate noncompetitive inhibition with respect to Mg^{2+} and uncompetitive inhibition with respect to $F16P_2$ (Fig. 3). As is evident from Fig. 3*A*, substrate inhibition increases significantly with rising inhibitor concentration. Data from Fig. 3*A* were fit to nine different

TABLE I
Hypothetical models of inhibition of FBPase by OC252

In the absence of inhibitor and substrate, all enzyme is in an $E{\cdot}(Mg^{2+})_2$ complex (conditions of saturating Mg^{2+}). Each model assumes a Hill coefficient of 2 for OC252 inhibition and rapid equilibrium kinetics, in which the conversion of $E{\cdot}(Mg^{2+})_2{\cdot}F16P_2$ to $E{\cdot}(Mg^{2+})_2{\cdot}F6P{\cdot}P_i$ is rate-limiting. The Michaelis equilibrium, $E{\cdot}(Mg^{2+})_2 + F16P_2 \Leftrightarrow E{\cdot}(Mg^{2+})_2{\cdot}F16P_2$, is common to all mechanisms, and is not included. M, S, and I below represent Mg^{2+}, $F16P_2$, and OC252, respectively. RMSD is the root mean squared deviation between observed velocities and those calculated from the model.

Model identifier	Equilibria & constants	Inhibition type	RMSD of fit
A	$E{\bullet}(M)_2 + 2I \Leftrightarrow E{\bullet}(M)_2{\bullet}I_2$; K_i	Competitive	2.609
B	$E{\bullet}(M)_2 + 2I \Leftrightarrow E{\bullet}(M)_2{\bullet}I_2$; K_i $E{\bullet}(M)_2{\bullet}I_2 + S \Leftrightarrow E{\bullet}(M)_2{\bullet}S{\bullet}I_2$; K_{is}	Competitive with induced substrate inhibition	0.235
C	$E{\bullet}(M)_2 + 2I \Leftrightarrow E{\bullet}(M)_2{\bullet}I_2$; K_i $E{\bullet}(M)_2{\bullet}S + 2I \Leftrightarrow E{\bullet}(M)_2{\bullet}S{\bullet}I_2$; K_i	Noncompetitive	0.686
D	$E{\bullet}(M)_2 + 2I \Leftrightarrow E{\bullet}(M)_2{\bullet}I_2$; K_i $E{\bullet}(M)_2{\bullet}S + 2I \Leftrightarrow E{\bullet}(M)_2{\bullet}S{\bullet}I_2$; K_i $E{\bullet}(M)_2{\bullet}S{\bullet}I_2 + S \Leftrightarrow E{\bullet}(M)_2{\bullet}S_2{\bullet}I_2$; K_{iis}	Noncompetitive with induced substrate inhibition	0.070
E	$E{\bullet}(M)_2 + 2I \Leftrightarrow E{\bullet}(M)_2{\bullet}I_2$; K_i $E{\bullet}(M)_2{\bullet}S + 2I \Leftrightarrow E{\bullet}(M)_2{\bullet}S{\bullet}I_2$; K_{ii}	Mixed	0.235
F	$E{\bullet}(M)_2 + 2I \Leftrightarrow E{\bullet}(M)_2{\bullet}I_2$; K_i $E{\bullet}(M)_2{\bullet}S + 2I \Leftrightarrow E{\bullet}(M)_2{\bullet}S{\bullet}I_2$; K_{ii} $E{\bullet}(M)_2{\bullet}S{\bullet}I_2 + S \Leftrightarrow E{\bullet}(M)_2{\bullet}S_2{\bullet}I_2$; K_{iis}	Mixed with induced substrate inhibition	0.026
G	$E{\bullet}(M)_2{\bullet}S + 2I \Leftrightarrow E{\bullet}(M)_2{\bullet}S{\bullet}I_2$; K_{ii}	Uncompetitive	0.234
H	$E{\bullet}(M)_2{\bullet}S + 2I \Leftrightarrow E{\bullet}(M)_2{\bullet}S{\bullet}I_2$; K_{ii} $E{\bullet}(M)_2{\bullet}S{\bullet}I_2 + S \Leftrightarrow E{\bullet}(M)_2{\bullet}S_2{\bullet}I_2$; K_{iis}	Uncompetitive with induced substrate inhibition	0.026
I	$E{\bullet}(M)_2{\bullet}S + 2I \Leftrightarrow E{\bullet}(M)_2{\bullet}S{\bullet}I_2$; K_{ii} $E{\bullet}(M)_2{\bullet}S{\bullet}I_2 + S \Leftrightarrow E{\bullet}(M)_2{\bullet}S_2{\bullet}I_2$; K_{iis} $E{\bullet}(M)_2{\bullet}S{\bullet}I_2 \Rightarrow$ products; k_{cat2}	Uncompetitive with induced partial substrate inhibtion	0.026

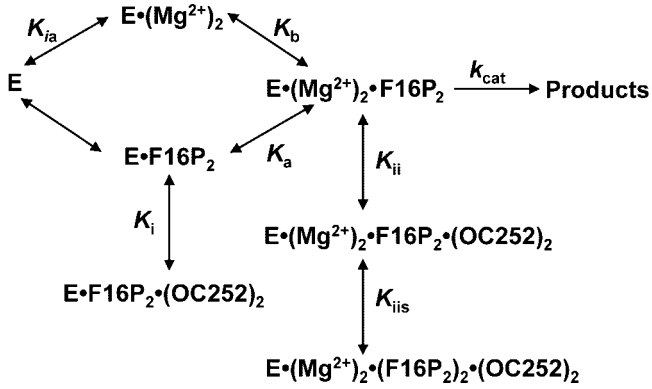

SCHEME I

TABLE II
Kinetic parameters determined by fits of Equations 3 and 4 to the data of Fig. 3. Maximum velocity is expressed in terms of the change in fluorescence (units not defined) with time

Parameter	Numerical value
Equation 3	
V_m	18.4 ± 0.3 Δ*F*/s
K_b	2.16 ± 0.08 μM
K_{ii}	25 ± 2 μM^2
K_{iis}	7.6 ± 1 μM
Equation 4	
V_m	17.1 ± 0.8 Δ*F*/s
K_a	0.38 ± 0.02 mM^2
K_i	3.65 ± 0.6 μM^2

kinetic models using the program DYNAFIT (27), combining mechanisms of competitive, noncompetitive, and uncompetitive inhibition by OC252, with and without pathways for inhibitor-induced substrate inhibition or partial inhibitor-induced substrate inhibition (Table I). (Inhibitor-induced substrate inhibition requires the binding of OC252 prior to the binding of the inhibitory $F16P_2$ molecule. Inhibitor-induced partial substrate inhibition allows turnover of the substrate-inhibited enzyme at a reduced maximal velocity.) All successful kinetic models include the association of two molecules of OC252 with an $E{\cdot}(Mg^{2+})_2{\cdot}F16P_2$ complex to form an $E{\cdot}(Mg^{2+})_2{\cdot}F16P_2{\cdot}(OC252)_2$ complex (uncompetitive inhibition with respect to $F16P_2$). The latter complex induces the formation of $E{\cdot}(Mg^{2+})_2{\cdot}(F16P_2)_2{\cdot}(OC252)_2$ (inhibitor-induced substrate inhibition). Parameters representing the formation of an $E{\cdot}(Mg^{2+})_2{\cdot}(OC252)_2$ complex (which would result in competitive, noncompetitive, or mixed inhibition with respect to $F16P_2$ and/or the turnover of the $E{\cdot}(Mg^{2+})_2{\cdot}(F16P_2)_2{\cdot}(OC252)_2$ complex (inhibitor-induced partial substrate inhibition) are not justified on the basis of *F* tests. Hence, model H of Table I represents the data at saturating Mg^{2+} with the fewest parameters. Scheme I then represents the kinetic mechanism of inhibition at all concentrations of the relevant ligands.

From Scheme I we derived the following relationship (Equation 2) assuming rapid-equilibrium kinetics under initial velocity conditions,

$$1/V = (1/V_m)(1 + K_a/A^2 + K_b/B + (K_{ia}K_b)/(A^2B) + (K_aI^2)/(K_iA^2) + (I^2/K_{ii})(1 + B/K_{iis})) \quad \text{(Eq. 2)}$$

where *A*, *B,* and I are concentrations of free Mg^{2+}, $F16P_2$, and OC252, respectively; V_m is the maximal velocity, and K_{ia}, K_a, K_b, K_i, K_{ii}, and K_{iis} are dissociations constants for two Mg^{2+} atoms from the $E{\cdot}(Mg^{2+})_2$ complex, for two Mg^{2+} atoms from the $E{\cdot}(Mg^{2+})_2{\cdot}F16P_2$ complex, for $F16P_2$ from the $E{\cdot}(Mg^{2+})_2{\cdot}F16P_2$ complex, for two OC252 molecules from the $E{\cdot}F16P_2{\cdot}(OC252)_2$ complex, for two molecules of OC252 from the $E{\cdot}(Mg^{2+})_2{\cdot}F16P_2{\cdot}(OC252)_2$ complex, and for the second (inhibitory) molecule of $F16P_2$ from the $E{\cdot}(Mg^{2+})_2{\cdot}(F16P_2)_2{\cdot}(OC252)_2$ complex, respectively. Equation 2 simplifies under conditions of saturating Mg^{2+} to Equation 3,

$$1/V = (1/V_m)(1 + K_b/B + (I^2/K_{ii})(1 + B/K_{iis})) \quad \text{(Eq. 3)}$$

which is used in the determination of V_m, K_b, K_{ii}, and K_{iis} from data in Fig. 3*A*. Under these conditions, $[F16P_2] \gg K_b$, Equation 2 simplifies to Equation 4,

$$1/V = (1/V_m)(1 + K_a/A^2 + (K_aI^2)/(K_iA^2) + (I^2/K_{ii})(1 + B/K_{iis})) \quad \text{(Eq. 4)}$$

which is used in the determination of V_m, K_a, and K_i from data in Fig. 3*B* using numerical values for K_{ii} and K_{iis} from Equation 3. Values for kinetic parameters are in Table II.

OC252 Complex of FBPase (Protein Data Bank Code 1Q9D)—Crystals grown in the presence of OC252 belong to the space group $P2_12_12$ (a = 58.86, b = 166.25, c = 80.27), and are isomorphous to those of AMP complexes of FBPase (17). Two subunits of FBPase are in the asymmetric unit of this crystal form. Cα coordinates of the independent subunits superimposed with a root mean square deviation of 0.38 Å, using a subset of residues (33−49, 75−265, and 272−330), which do not exhibit significant tertiary conformational differences between the T- and R-state subunits of FBPase (10). Regions of

TABLE III
Statistics of data collection and refinement for the OC252-FBPase complex

Resolution (Å)	2.35
No. measurements	94,949
No. unique reflections	28,849
Completeness of data	
Overall	87.5
Last shell (2.44-2.35 Å)	65.5
R_{sym}[a]	5.9
No. reflections in refinement[b]	27,163
No. atoms	5434
No. solvent sites	290
R-factor[c]	0.191
R_{free}[d]	0.246
Mean thermal parameters (Å^2)	
Protein	21.1
Mg^{2+}	22.1
F6P	24.5
P_i	50.1
OC252	13.6
Root mean square deviations	
Bond lengths (Å)	0.012
Bond angles (degree)	1.7
Dihedral angles (degree)	24.1
Improper angles (degree)	5.74

[a] $R_{sym} = \Sigma_j\Sigma_i|I_{ij} - \langle I_j\rangle|/\Sigma_i\Sigma_j I_{ij}$, where *i* runs over multiple observations of the same intensity and *j* runs over crystallographic unique intensities.
[b] All data are in the resolution range of 50-2.35 Å.
[c] *R*-factor = $\Sigma||F_{obs}| - |F_{calc}||/\Sigma|F_{obs}|$, where $|F_{obs}| > 0$.
[d] *R*-factor based upon 10% of the data randomly culled and not used in the refinement.

TABLE IV
Root mean squared deviations (in Å) in superpositions of C1-C2 subunits and tetramers (boldface) of FBPase

All superpositions employ Cα atoms of residues 33-49, 75-265, and 272-330. The *R*-state and T-state structures are from the Protein Data Bank, accession labels 1CNQ and 1EYK, respectively.

	T-state	OC252 complex
R-state	**2.71**/0.578	**2.16**/0.481
T-state		**0.703**/0.332

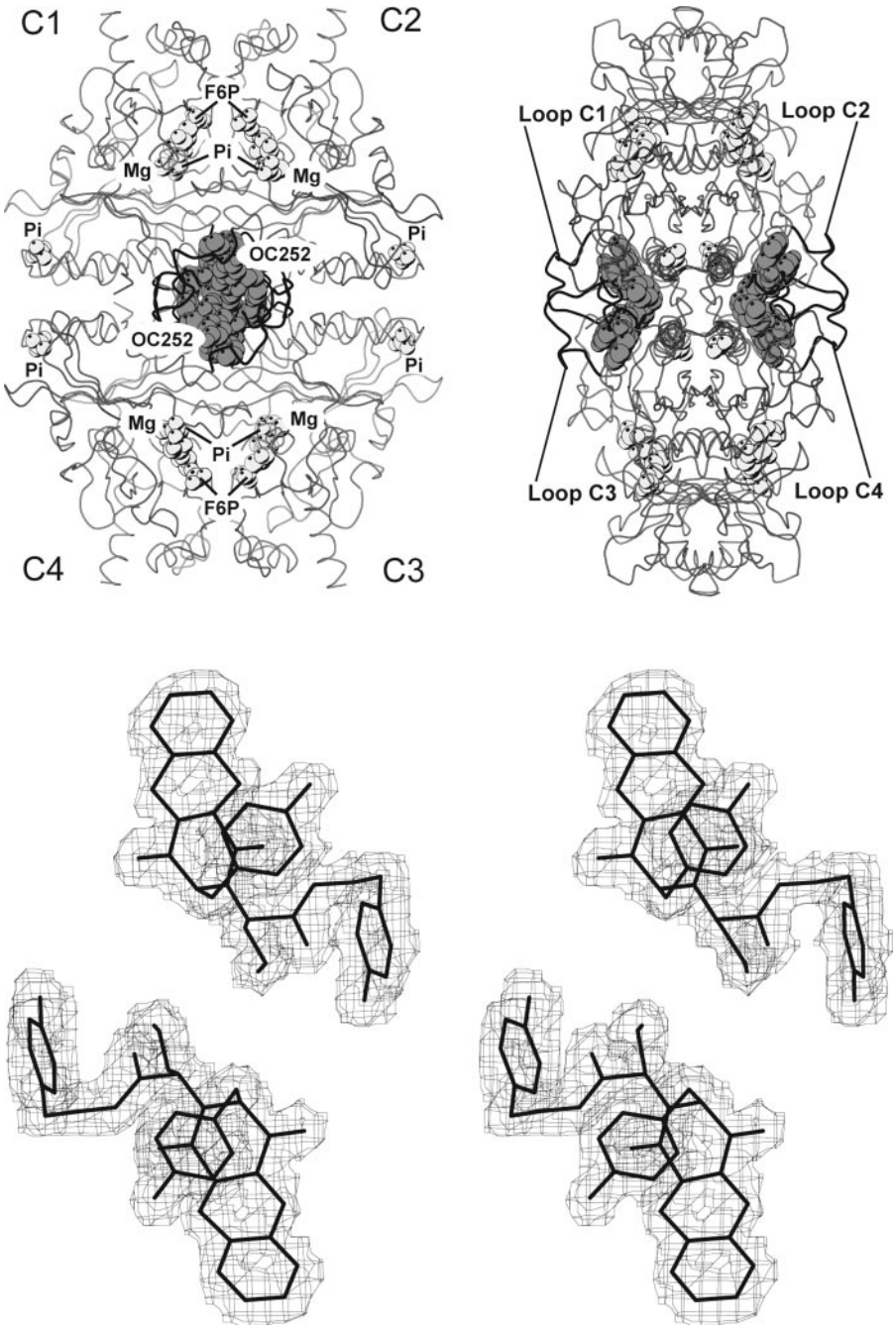

FIG. 4. **OC252-FBPase complex.** The *top panel* gives orthogonal views of the complex showing FBPase as a ribbon with atoms of Mg^{2+}, F6P, P_i, and OC252 as *spheres*. The *bottom panel* shows electron density covering a pair of OC252 molecules from an omit map contoured at a level of 1σ with a cut-off radius of 1 Å (*bottom*). This drawing was prepared with MOLSCRIPT (41).

weak or absent electron density include residues 1−8 and 63−70. The model begins at residue 9 and continues to the last residue of the sequence, but segment 63−70 is unreliable, as evidenced by high thermal parameters. Thermal parameters vary from 5 to 57 Å^2. As determined by PROCHECK (32), the model has stereochemistry generally comparable with that of structures derived from data of nominal resolution 2.0 Å. Statistics for data collection and refinement are in Table III, and an overview of the complex appears in Fig. 4.

Although the two subunits of the OC252 complex are similar, the ligation of each active site by metals differs. In the subunit labeled chain B, strong electron density is at metal site 1. The thermal parameter of Mg^{2+} at full occupancy here refines to a value of 10 Å^2, which is significantly less than the average value (20 Å^2) for atoms of the protein ligated to that metal. Hence Mg^{2+} and a heavier metal (Zn^{2+}, on the basis of prior experience (19)) probably co-occupy site 1 in chain B. Site 2 of chain B has diffuse electron density that may represent disordered water molecules or the combination of water molecules and Mg^{2+} at low occupancy; Mg^{2+} at full occupancy refined at metal site 2 with a thermal parameter of 32 Å^2. In the subunit labeled chain A, Mg^{2+} refines with thermal parameters of 18 and 29 Å^2 at sites 1 and 2, respectively. Metal site 2 in chain A may be occupied partially by Mg^{2+}. The conformations of side chains near metal site 2 also differ in each of the symmetry unique subunits of the crystal. In addition, molecules of P_i are at partial occupancy at each active site, but molecules of F6P are at full occupancy.

OC252 is arguably a highly constrained pseudo-tetrapeptide (Fig. 1); the first and fourth "residues" have tyrosyl side chains, a methylene group in residue *2* covalently bridges the phenylalanyl side chain to its amide nitrogen, and an *n*-propyl group is the side chain of residue *3*. The N-2 atom of OC252 corresponds to the backbone nitrogen atom of the first and third residues, and the terminal carboxyl group is absent. Atoms C-8, C-10, and C-12 have the L-configuration of a common amino

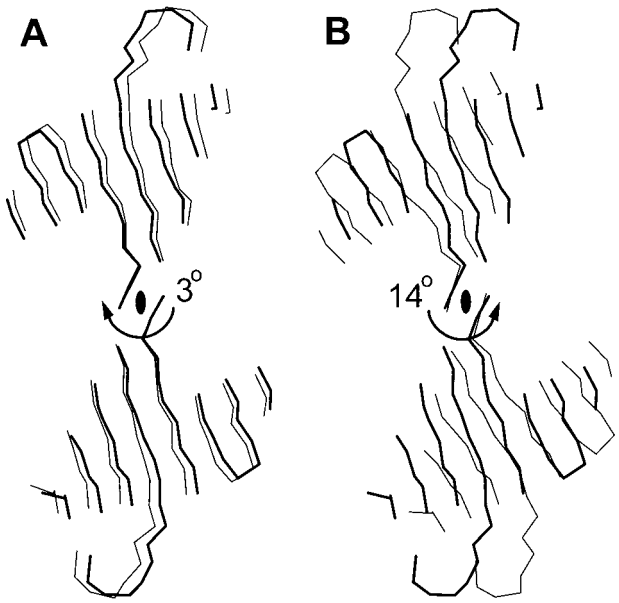

FIG. 5. **Superposition of the OC252 complex onto the T- and R-states of FBPase.** Cα atoms of residues 33−49, 75−265, and 272−330 of subunits C1 and C2 are the basis for superposition. Presented are displacements of Cα atoms in β-strands of the AMP domain of subunits C3 and C4 in the OC252 complex (*heavy lines*) relative to those of the T-state (*A*) and R-state (*B*).

acid. In their FBPase complex, two molecules of OC252 are in mutual contact, related to each other by the molecular 2-fold axis that projects through the face of the FBPase tetramer. Most of the contacts between inhibitor and protein are apolar; however, the phenol oxygen atoms of residues *1* and *4* of OC252 hydrogen-bond with backbone carbonyl 71 and the side chain of Asp^{187}, respectively. Furthermore, the C—O bond axis of backbone carbonyl 51 is normal to the plane defined by atoms C-8, N-2, C-11, and C-12 of OC252, with its oxygen atom 3.2 Å from atom N-2. The latter suggests an electronic resonance state of the bound OC252 molecule that stabilizes this close contact (Fig. 1).

Although the OC252 and AMP crystalline complexes are isomorphous, the two FBPase tetramers adopt different quaternary conformations. Superpositions of C1−C2 subunit pairs from the OC252, T-state, and R-state complexes give comparable root mean squared deviations (Table IV). (See Fig. 4 for the convention adopted in the labeling of subunits.) On the other hand, superpositions of tetramers give significantly larger deviations, suggesting different quaternary structures. Indeed, the C3−C4 subunit pair in the OC252 complex rotates ~14° relative to the C1−C2 subunit pair, falling some 3° short of the canonical T-state (Fig. 5). Hereafter, we refer to the quaternary state of FBPase induced by OC252 as the I-state.

The I-state must be due to the specific effects of the OC252 inhibitor. First, the conditions of crystallization for the T-, R-, and I-states of FBPase differ only by the presence or absence of allosteric effectors. The T-state crystallizes in the presence of AMP (17), the I-state in the presence of OC252, and the R-state in the absence of allosteric effectors (10, 17). Hence, ligation of FBPase by OC252 favors neither the T- nor R-state. OC252, however, stabilizes the disengaged conformation of loop 52−72, which prior to this work has been seen only in AMP-ligated complexes. Moreover, rotation of the side chain of His^{55} about its Cα−Cβ bond eliminates the only unfavorable contact between OC252 and the superimposed T-state. Hence, OC252 could bind to T-state FBPase in an AMP−OC252 complex. On the other hand, residues 51−56 of the engaged loop (a conformation observed only in the R-state) and the side chain of the poorly ordered Phe^{6} partially fill the OC252 binding pocket in the R-state. OC252 may still bind to the R-state enzyme, but at the very least loop 52−72 cannot be in its engaged conformation.

Although loop 52−72 represents the largest conformational difference at the tertiary level between subunits in the T- and R-states of FBPase, other significant changes occur in the vicinity of the AMP pocket. Helices H1 and H2 are ~2 Å closer to each other in the T-state than in the R-state, a difference attributed to the binding of AMP (14). Comparison of I-state and T-state subunits, however, presents a more complex scenario. Relative to the T-state, the binding site for the base of AMP is hindered sterically in the I-state. The interaction of backbone amide 17 and Thr^{31} with the 6-amino group of AMP would force the adenine base into an unfavorable contact (~2.5 Å) with the Cβ atom of Glu^{20} (Fig. 6). Evidently, a conformational change in the last two turns of helix H1 relaxes this unfavorable contact but in so doing perturbs Glu^{19} and Arg^{22}. The side chains of Glu^{19} and Arg^{22} are in contact with residues 26−28 of a neighboring subunit (C1−C4/C2−C3 interface). Residues 26−28 in turn hydrogen-bond with the 5′-phosphoryl group of AMP. Evidently, the collapse of helices H1 and H2 onto the AMP pocket then is complete in the I-state. Further progress toward the T-state then requires hydrogen bonds of the 6-amino group of AMP to force conformational changes at the C1−C4/C2−C3 interface.

DISCUSSION

OC252 and anilinoquinazolines (24) recognize a common site on FBPase, but the binding modes of these inhibitors differ substantially. Each inhibitor-type binds as a pair, but bound anilinoquinazoline and OC252 molecules have orthogonal orientations; two aniliquinazoline molecules overlap distinct moieties of a single OC252 molecule (Fig. 7). The quinazoline moiety of the anilinoquinazoline overlaps residues *1* and *2* of OC252, whereas the phenylthiazole moiety overlaps residue *3* of the other OC252 molecule. No part of the anilinoquinazoline molecule corresponds to residue *4* of OC252, the side chain of which hydrogen-bonds Asp^{187}. In fact, the phenylthiazole moiety through stacking interactions positions the side chain of His^{55} over the pocket occupied by the tyrosyl side chain of OC252 residue *4*. The anilinoquinazoline is roughly crescent-shaped; the ends of the crescent contact the surface of the FBPase tetramer with the curve of the crescent projecting outward. Residues *3* (*n*-propyl side chain) and *4* (tyrosyl side chain) of OC252, on the other hand, penetrate the interior of the tetramer. Hence, the number of contacts between OC252 and FBPase greatly exceeds that of the anilinoquinazoline. Each OC252 molecule interacts with residues from three of four subunits of FBPase, whereas each anilinoquinazoline molecule interacts with residues from a pair of subunits (Fig. 7). Curiously, despite all the differences above, both inhibitor types foster stabilizing interactions with backbone carbonyl 51 of FBPase. For the anilinoquinazoline, the hydroxyl group of the phenylthiazole moiety hydrogen-bonds directly with backbone carbonyl 51, whereas atom N-2 of the OC252 molecule is in a possible electrostatic contact with the oxygen atom of the backbone carbonyl 51.

Inhibitors of wild-type FBPases are either competitive (such as $F26P_2$) or noncompetitive (such as AMP) with respect to $F16P_2$. Uncompetitive inhibition of FBPase by OC252 with respect to the substrate is unusual but not unprecedented. The mutation of Arg^{49} to cysteine changes the kinetic mechanism of AMP inhibition with respect to $F16P_2$ from noncompetitive to uncompetitive, but retains the competitive mechanism of AMP inhibition with respect to Mg^{2+} (33). Evidently, AMP best inhibits Cys^{49} FBPase at low concentrations of Mg^{2+} and at high concentrations of $F16P_2$. The side chain of Arg^{49} partici-

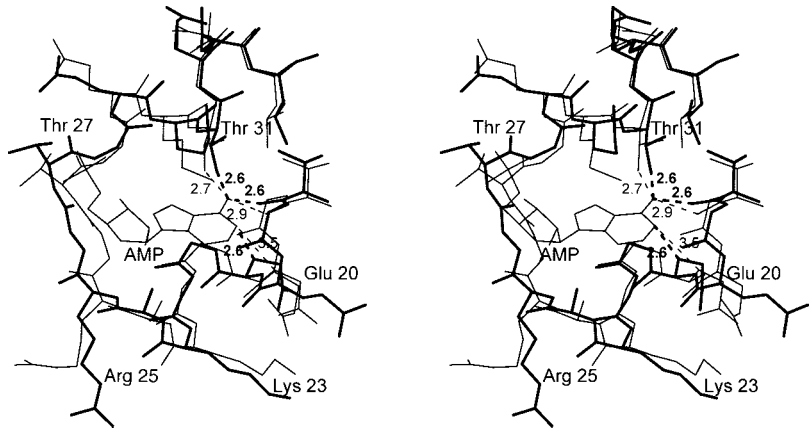

FIG. 6. **Stereoviews of the AMP binding pocket in different quaternary states of FBPase.** *Dashed lines* represent contacts between the AMP molecule and the T-state complex (*fine lines*) and the superimposed OC252 complex (*heavy lines*).

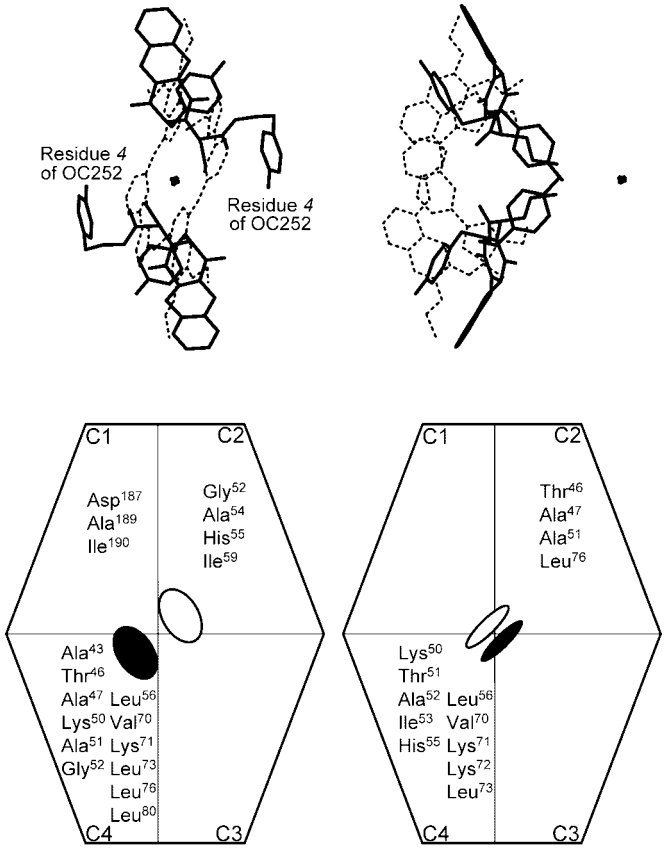

FIG. 7. **Comparison of the binding modes of OC252 and an anilinoquinazoline inhibitor.** The *top panel* shows the superposition of OC252 and anilinoquinazoline molecules (using FBPase tetramers as the basis of superposition) in orthogonal orientations corresponding to those of Fig. 4. The *bottom panel* lists residues that have atoms in contact with a single OC252 or anilinoquinazoline molecule. *Filled ellipses* represent the approximate location inhibitor molecules that give rise to the contacts. *Open ellipses* represent the relative position of the second molecule of the pair of bound inhibitors. Residues in contact are grouped within their respective subunits.

pates in several hydrogen-bonded interactions in the T-state of FBPase, and has low thermal parameters (20−25 Å^2), but is less ordered in the R-state, having thermal parameters of 40−45 Å^2 (17). The loss of Arg^{49} by mutation then may destabilize the T-state relative to the R-state. AMP may bind to Cys^{49} FBPase in the R-state but not cause a transition to the T-state. F16P$_2$ could stabilize an intermediate state of Cys^{49} FBPase that facilitates the binding of AMP, and indeed, F16P$_2$ and AMP in the absence of metals bind synergistically to wild-type FBPase (34). An uncompetitive pattern of inhibition would result then if subsequent AMP ligation of this F16P$_2$-stabilized state caused a transition to the T-state.

The quaternary state of FBPase stabilized by OC252 (the I-state) may be similar to this hypothetical F16P$_2$-stabilized state of Cys^{49} FBPase. First, uncompetitive inhibition by OC252 with respect to F16P$_2$ reflects binding synergism; ligation of the active site by F16P$_2$ enhances the affinity of OC252 for its binding site (see Scheme I). Moreover, the binding of OC252 induces F16P$_2$ inhibition (Fig. 3*B*). Binding synergism between OC252 and F16P$_2$ would occur if each ligand were to bind at distinct sites and stabilize a common conformational state of FBPase. Hence, the I-state observed in the OC252 complex may be similar to the quaternary state of FBPase in the presence of inhibitory concentrations of substrate. Ligation of FBPase by OC252 excludes the engaged conformation of loop 52−72, which is presumably required for catalysis. The I-state itself may disfavor the engaged conformation of loop 52−72, thereby accounting for the phenomenon of substrate inhibition of FBPase at concentrations of F16P$_2$ in excess of 30 μM.

The I-state may also be the basis for synergistic inhibition of FBPase by OC252 and F26P$_2$. Elevated levels of F26P$_2$ (200 μM) cause a transition from the loop-engaged R-state to a conformation similar but not identical to the T-state, as measured by fluorescence from a Trp^{57} reporter group (20). Perhaps high concentrations of F26P$_2$ stabilize the I-state, and indeed the tetramer does adopt the I-state in a preliminary crystal structure of an F26P$_2$-FBPase complex.[2] As OC252 and F26P$_2$ stabilize the same quaternary conformation by interactions at topologically distinct sites, they must exhibit functional synergism in rapid equilibrium kinetics.

An explanation of the synergism between AMP and OC252 is only slightly more complex. OC252 clearly excludes the engaged conformer of loop 52−72 and evidently stabilizes the disengaged loop present in the AMP complex of FBPase. Moreover, the I-state probably lies on or near the free energy pathway connecting the R- and T-states. So by stabilizing the I-state, OC252 does much of the work that AMP normally accomplishes in driving the R- to T-state transition.

But is the I-state of FBPase an appropriate target for the development of new drugs? Estimates of the free concentrations of F16P$_2$ in liver (~1 μM (35)) are well below those that cause substrate inhibition (30 μM and above) of FBPase. Similarly, concentrations of F26P$_2$ (200 μM) and products (250 μM) that stabilize the I-state in fluorescence experiments are far in excess of those *in vivo*. On the other hand, AMP and F26P$_2$ are the principal metabolic effectors of FBPase. Given that OC252 inhibits FBPase synergistically with AMP and F26P$_2$ at physiological concentrations of substrate, the central allosteric

[2] J.-Y. Choe and R. B. Honzatko, unpublished results.

pocket of FBPase could be an effective target, even if prevailing conditions *in vivo* do not favor the I-state.

Assays used to screen for potent inhibition of FBPase have employed concentrations of $F16P_2$ as high as 500 μM (24). These conditions exclude inhibitors that compete with $F16P_2$ and bias the screen in favor of ligands that inhibit FBPase only in the presence of bound $F16P_2$. Although this strategy has led to the discovery of molecules that do not bind to the active site, it has the disadvantage of selecting ligands that require high concentrations of $F16P_2$ for potent inhibition. For instance, $I_{0.5}$ is low (~6 μM) for OC252 in the presence of 100 μM $F16P_2$ but rises to 70 μM at a concentration of 2 μM $F16P_2$. Hence, an initial screen using high concentrations of $F16P_2$ may identify new leads that target the central allosteric site of FBPase, but further kinetic analysis at low concentrations of $F16P_2$ may be more appropriate in optimizing the lead compound as a potent inhibitor *in vivo*.

The above also assumes that no consequence beyond inhibition will result from the ligation of the central allosteric pocket of FBPase. Such an assumption, however, may be unwarranted. Available sequences of FBPase reveal Asp^{187} as an invariant residue. The mutation of Asp^{187} to alanine has only a modest effect on the functional properties of FBPase (36). Its mutation to phenylalanine has no greater effect on FBPase function than that due to the alanine mutation.[3] What selective pressure then retains aspartate at position 187 and is it just coincidence that OC252 hydrogen-bonds to this side chain? The conservation of Asp^{187} suggests a role in the recognition of a natural effector. Several reports (37–40) are in the literature, for instance, regarding interactions between FBPase and aldolase. The C-terminal residues of aldolase are putatively essential to these interactions, and the consensus sequences for both type A and B isozymes of aldolase end in tyrosine, which matches residue *4* of OC252. Hence, a potential drug may have to compete with a natural effector for the central allosteric pocket, or possibly FBPase itself may act as an effector in some other physiological process. Further clarification of these issues may be critical to the success of efforts to develop drugs that effectively target FBPase.

[3] C. Iancu and R. B. Honzatko, unpublished results.

REFERENCES

1. Benkovic, S. T., and de Maine, M. M. (1982) *Adv. Enzymol. Relat. Areas Mol. Biol.* **53,** 45–82
2. Tejwani, G. A. (1983) *Adv. Enzymol. Relat. Areas Mol. Biol.* **54,** 121–194
3. Van Schaftingen, E. (1987) *Adv. Enzymol. Relat. Areas Mol. Biol.* **59,** 45–82
4. Pilkis, S. J., El-Maghrabi, M. R., and Claus, T. H. (1988) *Annu. Rev. Biochem.* **57,** 755–783
5. Okar, D. A., and Lange, A. J. (1999) *Biofactors* **10,** 1–14
6. Pilkis, S. J., El-Maghrabi, R. M., McGrane, M. M., Pilkis, J., and Claus, T. H. (1981) *J. Biol. Chem.* **256,** 3619–3622
7. Nimmo, H. G., and Tipton, K. F. (1975) *Eur. J. Biochem.* **58,** 567–574
8. Liu, F., and Fromm, H. J. (1988) *J. Biol. Chem.* **263,** 9122–9128
9. Scheffler, J. E., and Fromm, H. J. (1986) *Biochemistry* **25,** 6659–6665
10. Choe, J.-Y., Poland, B. W., Fromm, H. J., and Honzatko, R. B. (1998) *Biochemistry* **33,** 11441–11450
11. Stone, S. R., and Fromm, H. J. (1980) *Biochemistry* **19,** 620–625
12. Ke, H., Zhang, Y., Liang, J.-Y., and Lipscomb, W. N. (1991) *Proc. Natl. Acad. Sci. U. S. A.* **88,** 2989–2993
13. Liu, F., and Fromm, H. J. (1988) *J. Biol. Chem.* **19,** 9122–9128
14. Zhang, Y., Liang, J.-Y., Huang, S., and Lipscomb, W. M. (1994) *J. Mol. Biol.* **244,** 609–624
15. Nelson, S. W., Kurbanov, F., Honzatko, R. B., and Fromm, H. J. (2001) *J. Biol. Chem.* **276,** 6119–6124
16. Xue, Y., Huang, S., Liang, J.-Y., Zhang, Y., and Lipscomb, W. N. (1994) *Proc. Natl. Acad. Sci. U. S. A.* **91,** 12482–12486
17. Choe, J.-Y., Fromm, H. J., and Honzatko, R. B. (2000) *Biochemistry* **39,** 8565–8574
18. Choe, J.-Y., Nelson, S. W., Fromm, H. J., and Honzatko, R. B. (2003) *J. Biol. Chem.* **278,** 16008–16014
19. Choe, J.-Y., Iancu, C. V., Fromm, H. J., and Honzatko, R. B. (2003) *J. Biol. Chem.* **278,** 16015–16020
20. Nelson, S. W., Choe, J.-Y., Iancu, C. V., Honzatko, R. B., and Fromm, H. J. (2000) *Biochemistry* **39,** 11100–11106
21. Wen, J., Nelson, S. W., Honzatko, R. B., Fromm, H. J., and Petrich, J. W. (2001) *Photochem. Photobiol.* **74,** 679–685
22. Ke, H. M., Thorpe, C. M., Seaton, B., Lipscomb, W. N., and Marcus, F. (1990) *J. Mol. Biol.* **212,** 513–539
23. Lu, G., Stec, B., Giroux, E. L., and Kantrowitz, E. R. (1996) *Protein Sci.* **5,** 2333–2342
24. Wright, S. W., Carlo, A. A., Carty, M. D., Danley, D. E., Hageman, D. L., Karam, G. A., Levy, C. B., Mansour, M. N., Mathiowetz, A. M., McClure, L. D., Nestor, N. B., McPherson, R. K., Pandit, J., Pustilnik, L. R., Schulte, G. K., Soeller, W. C., Treadway, J. L., Wang, I.-K., and Bauer, P. H. (2002) *J. Med. Chem.* **45,** 3865–3877
25. Laemmli, U. K. (1970) *Nature* **227,** 680–685
26. Bradford, M. M. (1976) *Anal. Biochem.* **72,** 248–252
27. Kuzmic, P. (1996) *Anal. Biochem.* **237,** 260–273
28. Howard, A. J., Nielsen, C., and Xuong, N. H. (1985) *Methods Enzymol.* **114,** 452–472
29. McRee, D. E. (1992) *J. Mol. Graphics* **10,** 44–46
30. Brünger, A. T., Adams, P. D., Clore, G. M., DeLano, W. L., Gros, P., Grosse-Kunstleve, R. W., Jiang, J.-S., Kuszewski, J., Nilges, M., Pannu, M. S., Read, R. J., Rice, L. M., Simonson, T., and Warren, G. L. (1998) *Acta Crystallogr. Sect. D Biol. Crystallogr.* **54,** 905–921
31. Engh, R. A., and Huber, R. (1991) *Acta Crystallogr. Sect. A* **47,** 392–400
32. Laskowski, R. A., Mac Arthur, M. W., Moss, D. S., and Thornton, J. M. (1993) *J. Appl. Crystallogr.* **26,** 283–291
33. Shyur, L.-F., Poland, B. W., Honzatko, R. B., and Fromm, H. J. (1997) *J. Biol. Chem.* **272,** 26295–26299
34. McGrane, M. M., El-Maghrabi, M. R., and Pilkis, S. J. (1983) *J. Biol. Chem.* **258,** 10445–10454
35. Lawson, J. W. R., Guynn, R. W., Cornell, N., and Veech, R. L. (1976) in *Gluconeogenesis: Its Regulation in Mammalian Species* (Hanson, R. W., and Mehlman, Y. A., eds) pp. 481–512, John Wiley & Sons, Inc., New York
36. Lu, G., Giroux, E. L., and Kantrowitz, E. R. (1997) *J. Biol. Chem.* **297,** 5076–5081
37. MacGregor, J. S., Singh, V. N., Davoust, S., Melloni, E., Pontremoli, S., and Horecker, B. L. (1980) *Proc. Natl. Acad. Sci. U. S. A.* **77,** 3889–3892
38. Pontremoli, S., Melloni, E., and Horecker, B. L. (1983) *Biochem. Soc. Trans.* **11,** 241–244
39. Rakus, D., and Dzugaj, A. (2000) *Biochem. Biophys. Res. Commun.* **275,** 611–616
40. Moorhead, G. B. G., Hodgson, R. J., and Plaxton, W. C. (1994) *Arch. Biochem. Biophys.* **312,** 326–335
41. Kraulis, J. (1991) *J. Appl. Crystallogr.* **24,** 946–950

Inhibition of Fructose-1,6-bisphosphatase by a New Class of Allosteric Effectors

Jun-Young Choe, Scott W. Nelson, Kristen L. Arienti, Frank U. Axe, Tassie L. Collins, Todd K. Jones, Rachel D. A. Kimmich, Michael J. Newman, Karl Norvell, William C. Ripka, Suzanne J. Romano, Kevin M. Short, Deborah H. Slee, Herbert J. Fromm and Richard B. Honzatko

J. Biol. Chem. 2003, 278:51176-51183.
doi: 10.1074/jbc.M308396200 originally published online October 6, 2003
